Sustainable Energy & Fuels

Accepted Manuscript

Volume 1 | Number 1 | 2017 | Pages 1–100

Sustainable Energy & Fuels

Interdisciplinary research for the development of sustainable energy technologies
rsc.li/sustainable-energy

ROYAL SOCIETY OF CHEMISTRY

175 YEARS

This is an Accepted Manuscript, which has been through the Royal Society of Chemistry peer review process and has been accepted for publication.

Accepted Manuscripts are published online shortly after acceptance, before technical editing, formatting and proof reading. Using this free service, authors can make their results available to the community, in citable form, before we publish the edited article. We will replace this Accepted Manuscript with the edited and formatted Advance Article as soon as it is available.
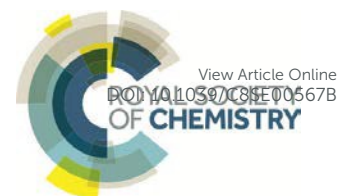
You can find more information about Accepted Manuscripts in the **author guidelines**.

ROYAL SOCIETY OF CHEMISTRY

rsc.li/sustainable-energy

Article type: Full paper

Sustainable Energy & Fuels
Interdisciplinary research for the development of sustainable energy technologies

Website rsc.li/sustainable-energy
Impact factor Pending

Journal expectations To be suitable for publication in *Sustainable Energy & Fuels* articles must significantly contribute to the development of sustainable energy technologies.

Article type: Full paper Original scientific work that has not been published previously. Full papers do not have a page limit and should be appropriate in length for scientific content.

Journal scope Visit the *Sustainable Energy & Fuels* website for additional details of the journal scope and expectations.

Sustainable Energy & Fuels publishes high quality scientific research that will drive development of sustainable energy technologies, with a particular emphasis on innovative concepts and approaches.

The journal is an essential resource for energy researchers and cuts across major disciplines – chemistry, physics, biology, materials science and engineering – covering evolving and emerging areas, including:

- Solar energy conversion including photovoltaics and artificial photosynthesis
- Energy storage including batteries and supercapacitors
- Catalysis for energy technologies, including the sustainable synthesis of fuels and chemicals
- Fuel cells
- Hydrogen production, storage and distribution
- Carbon capture, storage and utilisation, including chemicals from carbon dioxide
- Bioenergy including biofuels, biomass conversion and fuels from living organisms
- Other sustainable energy conversion technologies including thermochemical, piezoelectric and thermoelectric materials and devices

Reviewer responsibilities Visit the Reviewer responsibilities website for additional details of the reviewing policy and procedure for Royal of Society of Chemistry journals.

When preparing your report, please:
- Focus on the originality, importance, impact and reliability of the science. English language and grammatical errors do not need to be discussed in detail, except where it impedes scientific understanding.
- Use the journal scope and expectations to assess the manuscript's suitability for publication in *Sustainable Energy & Fuels.*
- State clearly whether you think the article should be accepted or rejected and include details of how the science presented in the article corresponds to publication criteria.
- Inform the Editor if there is a conflict of interest, a significant part of the work you cannot review with confidence or if parts of the work have previously been published.

Thank you for evaluating this manuscript, your advice as a reviewer for *Sustainable Energy & Fuels* is greatly appreciated.

Comparative study of light and thermal induced degradation for both fullerene and non-fullerene based organic solar cells

Leiping Duan[*,†], Haimang Yi[†], Yu Zhang[†], Faiazul Haque[†], Cheng Xu[†], Ashraf Uddin[*,†]

AUTHOR ADDRESS

†School of Photovoltaic and Renewable Energy Engineering, University of New South Wales, Sydney, NSW 2052, Australia

Corresponding authors

*Leiping Duan (Leiping.duan@unsw.edu.au)

*Ashraf Uddin (a.uddin@unsw.edu.au)

Abstract

Solution processed organic solar cells (OSCs) have becoming a promising renewable energy technology these years. The fast inital degradation which cause a performance reduction at a very intial stage for OSCs needs to be understood and investigated thoroughly. In this work, for the first time we have conducted a comparative study of light and thermal induced degradation during the burn-in process. As revealed in the estimation of Urbach energy, both light and thermal degradation created an increased energetic disorder. However, the following characterisaiton such as steady-state photoluminescence (PL), time-resolved photoluminescence (TRPL) and capacitance-voltage (C-V) indicates that the mechanism behind these two types of degradation is very different. The loss in light degradation was found more related to its degraded energy transfer ability, exition dissociation ability and increased non-radiative recombination. Whereas, the loss in thermal degradation was found more related to the reduced current extraction ability and increased leakage current.

Keywords: Organic solar cells, stability, fast inital degradation, non-fullerene acceptor

1. Introduction

Bulk heterojunction (BHJ) organic solar cells (OSCs), possessing advantages of simple and cheap fabrication, light-weight, semitransparent and flexible, have attracted many research attentions these years [1-4]. Recently, non-fullerene acceptor based organic solar cells are becoming the research hot spot [5]. Compared to coventional fullerene acceptors, non-fullerene acceptors have advantages such as stronger light absoring ability, tunable energy level and variable molecular structures [6-8]. Poly[4,8-bis(5-(2-ethylhexyl)thiophen-2-yl)benzo[1,2-b;4,5-b']dithiophene-2,6-diyl-alt-(4-(2-ethylhexyl)-3-fluorothieno[3,4-b]thiophene-)-2-carboxylate-2-6-diyl)] (PTB7-Th) is a widely applied low bandgap polymer donor material which showed a good compatibility with both classic fullerene and non-fullerene acceptor materials - [6,6]-Phenyl-C71-butyric acid methyl ester ($PC_{71}BM$) and 3,9-bis(2-methylene-(3-(1,1-dicyanomethylene)-indanone))-5,5,11,11-tetrakis(4-hexylphenyl)-dithieno[2,3-d:2′,3′-d′]-s-indaceno[1,2b:5,6-b′]dithiophene (ITIC) [9]. With the development of novel organic materials synthesis and device processing technology, the power conversion efficiency (PCE) of OSCs have overpassed 14% for single junction devices and 17% for tandem devices to date [10-14].

OSCs emerged as a promising renewable energy technology towards commercialisation. Nevertheless, besides reaching the high PCE, stability issue is a critical barrier for commercialisation. It was found that OSCs usually showed a dramatic performance degradation at the initial stage of the device operation [15-18]. This rapid reduction is defined as the"fast inital degradation", which is responsible for a significant loss in OSCs [19]. Commonly, a burn-in test is required for most of the photovoltaic devices to ensure its reliability [20]. For the future application, the fast inital degradation of organic solar cells also needs to be well understood and investigated. There are many factors contributing to the degradation of OSCs including the chemical instability, oxidation, interficial degradation, thermally induced changes, light-induced instaility and so on [21-24]. Different factors may attribute to various failure mechanism. To date, many studies have investigated the mechianism behind the light-induced fast inital degradation, also called burn-in photo degradation [16, 18]. Upama et al. reported that the formation of sub bandgap trap states is the main reason for the burn-in photo degradation in PTB7:$PC_{71}BM$ fullerene based organic solar cells [18]. Similarly, the trap-mediated charge recombination was found as the dominate burn-in photo degradation mechanism in non-fullerene based PBDB-T:ITIC deivces [17]. Nevertheless, rarely have researchers studied the fast inital degradation that results from other factors and did a

comparative study. Many stability studies only investigated the single factor such as thermal or air for a long term and lack of a detailed mechanism analysis [25-28]. Under this circumstance, more detailed and comparative stability studies are needed in this field. In addtion to the light, thermal-induced degradation is an innegligible part of fast inital degradation. To fully investigate the meachansim behind the fast inital degradation, a comparative analysis bewteen the fast inital photo degradation and fast inital thermal degradation for organic solar cells is inevitable.

In present works, we evaluated the fast inital photo degradation and fast inital thermal degradation for both PTB7-Th:PC$_{71}$BM based fullerene and PTB7-Th:ITIC based non-fullerene OSCs and we firstly compared this two types of degradation. Similar PCE reduction was observed for both photo-degraded devices and thermal-degraded devices. However, photo-degraded devices showed a higher open circuit voltage (V$_{oc}$) loss while thermal degraded devices showed a higher short circuit current (J$_{sc}$) loss. To investigate the rootcause of the difference, characterisations such as external quantum efficiency (EQE), photoluminescence (PL), capacitance-voltage (C-V) and atomic force microscopes (AFM) measurements were conducted. We determined the Urbach energy from the tail region of the EQE spectrum and estimated the carrier recombination resistance from the diode ideality factor. As results, the degradation mechansim was found different between the fast inital photo-degradation and thermal degradation. An increase in Urbach energy was observed for both photo-degraded and thermal-degraded devices with a similar extent. This indicates a larger energtic disorder in the device. The loss in fast inital photo degradation was found more related to its degraded energy transfer ability, exition dissciation ability and increased non-radiative recombination. Differently, the loss in fast inital thermal degradation was found more related to its decreased current extraction ability and increased leakage current.

2. Experimental Details

2.1 Materials Preparation

The pre-patterned ITO glasses with the area of 12 mm × 12 mm were purchased from Lumtec. The chemical materials PTB7-Th and ITIC were purchased from Solarmer. The chemical materials PC$_{71}$BM was purchased from 1-Material. The chemical material, zinc oxide nanoparticles, reagent alcohol (anhydrous, <0.003% water), chlorobenzene (99.8%), 1,8-diiodooctane, and MoO$_3$ were purchased from Sigma-Aldrich.

2.2 Device Fabrication

In this paper, we used an inverted device structure of ITO Glass/ZnO/PTB7-Th:ITIC or PTB7-Th:PC71BM /MoO$_3$/Ag. ITO glass substrate was cleaned through soapy deionised (DI) water, pure DI water, acetone and isopropanol by 10 min ultrasonication in sequence. The ZnO nanoparticle solution (3%) was made by adding 50 uL zinc dispersion into 1622uL reagent alcohol. The ZnO nanoparticles solution is stirred overnight in the N$_2$ filled glove box and then spin-coated on the top of the cleaned ITO glass with a spin rate of 5000 rpm for the 60 s. After coated ZnO solution, all the samples were annealed at 120 ℃ on the hot plate inside the N$_2$ filled glove box for 10 min. The PTB7-Th:PC71BM active layer solutions were made by 10 mg PTB7-Th and 15 mg PC71BM with a 1:1.5 wt ratio in a 25 mg/mL chlorobenzene solution with 3 vol% DIO. The PTB7-Th:ITIC active layer solutions were made by 10 mg PTB7-Th, 15 mg ITIC with a 1:1.5 wt ratio in a 25 mg/mL chlorobenzene without DIO addation. The active layer solution was stirred overnight inside an N$_2$-filled glovebox and then spin-coated at a rate of 1800 rpm for 2 min. on samples to reach a 100 nm thickness. After that, the coated samples were put into a vacuum chamber at a pressure of 10^{-5} Pa. The 10 nm thick film of MoO$_3$ and 100 nm thick film of silver was deposited to the sample surface through a shadow mask by thermal evaporation. The device area fabricated was 0.045 cm^2.

2.3 Device Characterization

Fresh samples are stored in an N$_2$-filled glove box to avoid degradation before characterisations. For photo-degraded samples, it has been put under one-sun test condition at ambient for 5 hours. For thermal-degraded samples, it has been put on an 85 ℃ hot plate for 5 hours in ambient condition. The current density-voltage (J–V) measurements were conducted by using a solar cell I–V testing system from PV Measurements, Inc. (using a Keithley 2400 source meter) under illumination power of 100 mW/cm^2 by an AM 1.5G solar simulator. The device temperature was measured by GM1350 50:1 LCD infrared thermometer digital gun and maintained at around 25 ℃. An Autolab PGSTAT-30 was used for the capacitance-voltage (C-V) characterisation and electrochemical impedance spectroscopy (EIS). This characterisation was conducted inside the glove box with a frequency range of 10^6-100 Hz by using a frequency analyser module. A QEX10 spectral response system from PV measurements was used as a characterisation machine for external quantum efficiency (EQE) measurements. The optical characterisation was conducted by a UV–VIS–NIR spectrometer (Perkin Elmer–Lambda 950).

A Bruker Dimension ICON SPM with a scan size of "5 μm × 5 μm", the scan rate of 0.512 Hz was used as the atomic force microscopy (AFM) to characterise the film surface morphology. Scanning electron microscopy (SEM) images were taken using a Nano SEM 230 system. The micro-photoluminescence (μPL) characterisation was conducted on a self-developed μPL system. The sample was excited by a pulsed OPO laser at 532 nm. For steady state spectral PL, the signal was detected by Glacier X TE Cooled CCD Spectrometer with a detection range of 200nm to 1050nm. For time-resolved PL (TRPL), the signal was detected by id110 VIS 100MHz Photon Detector operated in free running mode.

3.   Results and Discussions

In this work, all devices are fabricated with the inverted structure as shown in Figure 1 (a) inside the N_2 filled glove box. PTB7-Th, ITIC and $PC_{71}BM$ are the three organic materials that used to fabricate PTB7-Th:$PC_{71}BM$ fullerene based and PTB7-Th:ITIC non-fullerene based active layers. The chemical structure and energy level of these three materials were shown in Figure 1 (b) and (d) and the normalized absorbance of the two active layers are shown in Figure 1 (c). Organic solar cells characterized immediately after the fabrication are called "fresh" devices. These devices are then divied into two groups for fast inital degradation analysis. To evaluate the fast inital photo degradation in ambient condition, fresh devices were exposed to continuous one-sun test conditon for 5 hours in ambient condition to become so called "photo-degraded" devices [17]. To evaluate the fast inital thermal degradation, fresh devices were put on a hot plate with 85 ℃ under the dark condition for 5 hours in ambient condition to become so called "thermal-degraded" devices [15]. The photovoltaic parameters including V_{oc}, J_{sc}, fill factor (FF), PCE, series resistance (R_s) and shunt resistance (R_{sh}) of those devices were evaluated at a regular interval of 1 hour during the degradation process. The current density to voltage (J-V) curves of fresh, photo-degraded and thermal-degraded for both fullerene and non-fullerene based devices were displayed in Figure 2, and the corresponding photovoltaic parameters extracted from Figure 2 were listed in Table 1.

The photovoltaic parameters for PTB7-Th:$PC_{71}BM$ fullerene based device and PTB7-Th:ITIC non-fullerene based devices are similar, with a slightly higher J_{sc} value in fullerene based devices (14.67 ± 0.67 mA/cm^2) compared to that of non-fullerene based devices (13.13 ± 0.73 mA/cm^2). The highest PCE of 8.08% and 7.31% were achieved by the fullerene based and non-fullerene based device, respectively. From the fast inital degradation perspective, both fullerene

and non-fullerene devices degraded dramatically within 5 hours. Fullerene devices showed a slightly higher resistivity to burn-in process after 5 hours, with 73% and 71% of PCE maintained after the fast inital photo degradation and thermal degradation, and while non-fullerene based devices maintained only 57% and 63% of PCE after the degradation. Figure 3 (a)-(l) displayed the fast inital aging curves of all photovoltaic parameters including V_{oc}, J_{sc}, FF, PCE, R_s and R_{sh} for both fullerene based and non-fullerene based devices for 5 hours, and Table S1 and S2 showed the corresponding values of those photovoltaic paramters. From Figure 3 (g) and (h), the PCE loss after 5 hours in fast inital photo degradation and thermal degradation was found very similar for both types of devices, while the degradation trend in 5 hours was found different.

From photo-degradation perspective, non-fullerene based devices showed a typical burn-in degradation where the PCE showed a significant drop in the initial 1 hour following by a stabilization regime. While for fullerene based devices, the burn-in degradation regime is not apparent that the PCE decreased continuously over 5 hours. From thermal degradation perspective, both fullerene and non-fullerene based devices showed the burn-in process with a significant PCE drop within the initial 1 hour. Differently, the fullerene based devices showed a PCE recovering trend for the following 4 hours. As similar recovering trends were also observed in the degradation curve of the fill factor, shunt resistance and series resistance for fullerene based devices, the recovering of these three factors can be the main reason for the PCE recovering trend. Since all devices used the same device structure and the same donor material in this study, the degradation difference between the fullerene and non-fullerene based devices mainly results from the degradation in the active layer which is related with the morphology change and the molecular structure of the acceptor. Compared to fullerene acceptor $PC_{71}BM$, non-fullerene acceptor ITIC owns four 4-hexylphenyl groups which can restrict molecular planarity, aggregation and large phase separation [9]. Thermal treatment was proved can cause aggregation and larger domain size to reach higher carrier mobility for PTB7-Th:$PC_{71}BM$ devices which may be the root reason for the PCE recovering observed [29].

From Figure 3 (a) - (d), it is easy to observe that, the degradation of V_{oc} and J_{sc} is different in the fast inital photo degradation and thermal degradation, where photo-degraded devices have a higher V_{oc} loss and thermal-degraded devices have a higher J_{sc} loss. From Figure 3 (i) – (l), it can be seen that the degradation of the internal resitance is also different in the photo degradatio nand thermal degradation. After 5 hours degradation, thermal-degraded devices showed a higher shunt resistance loss while photo-degradation devices showed a higher series

resistance increase. Thus, the degradation mechanism of fast inital photo degradation and thermal degradation can be very different.

To investigate the mechanism behind the fast inital photo degradation and thermal degradation, EQE measurements with high sensitivity were conducted for fresh, photo-degraded and thermal-degraded devices. It is worth to meantion that all measurements were conducted under constant one sun light bias as the variation of the sun light bias will casue the variation in the EQE results[30]. Figure 4 (a) and (b) depicted the curves of EQE versus the photon energy for fullerene based and non-fullerene based devices, respectively. Since the photocurrent spectrum response of the polymer donor PTB7-Th is up to 1.6 eV [31], the photocurrent response of the device higher than 1.6 eV is more related to the excitation of the polymer chains, and the photocurrent response of the device lower than 1.6 eV is more corresponded with the excitation of the charge transfer (CT) states [32]. Urbach energy was then determined with the absoprtion tail (also called the Urbach tail) below 1.6 eV of the device by using the following equation [33, 34]:

$$EQE(E) \propto \alpha(E) \propto \exp\left(\frac{E}{E_U}\right) \qquad (1)$$

where E represents the photon energy, α represents the light absorbing coefficient and E_U is the estimated Urbach energy [33-36]. The extracted Urbach energy for both fullerene and non-fullerene, fresh, photo-degraded and thermal-degraded devices was listed in Table 2. It was found that both photo-degraded devices and thermal-degraded devices showed a similarly increased Urbach energy when compared to fresh devices. A higher Urbach energy usually indicates a higher energetic disorder with increased states in the bandgap of the active layer which can cause a reduction in the photovoltaic performance via trap mediated charge recombination [37]. Thus, the increased energetic disorder with higher trap mediated charge recombination was found as a common reason for both fast inital photo degradation and thermal degradation. Figure 4 (c) and (d) showed the EQE curves over the light wavelength range from 300 nm to 850 nm for both fullerene and non-fullerene based devices. For both types of devices, thermal-degraded devices exhibited a relatively higher EQE reduction than photo-degraded devices when compared to fresh devices, which is consistent with the observation of J_{sc} loss from J-V characterisation.

Dark J-V characterisation was then conducted to futher analyze the current loss in both fast inital photo and thermal degradation. The obtained dark J-V curves were shown in Figure 5 (a) and (b) for fullerene and non-fullerene based devices, respectively. It was clear to see that the

leakage current of photo-degraded and thermal-degraded devices increased for both types of devices under the reverse bias conditon compared to fresh devices. Moreover, the thermal-degraded devices showed a higher increasement than the photo-degraded devices. The high leakage current usually indicates a high shunt possibility which is responible for the low J_{sc} in and a low shunt resistance which is responsible for the low FF in OSCs [38]. Herein, the observation from leakage current explained the higher J_{sc} loss in thermal-degraded devices and in coherent with the observed higher shunt resistance loss from J-V charactherization. The results from dark J-V measurements proved that fast inital thermal degradation is more responsible for the increased shunt resistance and higher shunt probability in OSCs.

On the other hand, a saturation current density (J_{sat}) with charge carrier extraction possibility (P) analysis was performed for both fullerene and non-fullerene based, fresh, photo-degraded and thermal-degraded deivces. The photocurrent density (J_{ph}) to the effective voltage (V_{eff}) curves were shown in Figure 6. The J_{ph} and V_{eff} are calculated by using equations below [39]:

$$J_{ph} = J_L - J_D \qquad\qquad\qquad (2)$$

$$V_{eff} = V_{oc} - V_{bias} \qquad\qquad\qquad (3)$$

where J_L is the light current density under one-sun test condtion, J_D is the dark current density under the dark test condition, and V_{bias} is the externally applied voltage bias. When the V_{eff} is higher than 1.0 V, the assumption that all the generated excitons in the active layer are dissociated and collected can be made. In the meantime, the photocurrent density (J_{ph}) can be assumed equal to the saturation current density (J_{sat}) which is only restricted by the absorption of incident photons. The charge carriers extraction possibility (P) is then extracted by calculating the ratio of J_{sc} to J_{sat} which can reasonably explain the current loss during the current extraction process [40]. Table 3 presents the J_{sat} and estimated P value for all devices. It was found that, for both fullerene and non-fullerene based, the thermal-degraded devices showed a higher reduction in J_{sat} and P values than the photo-degraded devices when comparing to fresh devices which revealed that fast initial thermal degradation has a more negative effect on current extraction process in OSCs compared to fast inital photo degradation. Charge extraction process in OSCs is commonly related to the charge collection at the interface bewteen charge transport layers and active layer [41, 42]. The low charge collection at the interface usually results from the poor surface contact with occurred shunt condtion and indicates a low shunt resistance [43]. Thus, the results from the $J_{ph} - P$ analysis was found also consistent with the observed higher shunt resistance loss in J-V characterization.

To investigate the electrical properties changing in fast inital degradation, C-V characterisation was conducted. Figure 7 (a) and (b) displayed the Mott Schottky (MS) curves at a frequency of 1 kHz for fullerene and non-fullerene based devices. When the applied voltage bias is lower than 0.0 V, the assumption that the active layer is entirely depleted can be made [44]. Under this condtion, the dielectric constant of the device can be estimated by using the capacitance at 0.0 V bias with the equation below [45]:

$$C = \varepsilon_r \varepsilon_0 \frac{A}{d} \tag{4}$$

where A is the area of the device which is 0.045 cm^2 in this study, d is the thickness of the active layer which is around 100 nm for all devices, ε_o represents the vacuum permittivity of 8.854×10^{-12} F m^{-1}, and ε_r is the estimated relative dielectric constant. As known the dielectric constant, the colombic capture radius (R_c) which decribes the charge dissociation process can be estimated by using the following equation [46]:

$$R_c = \frac{e^2}{4\pi\varepsilon_r\varepsilon_0 kT} \tag{5}$$

where k is the Boltzmann constant, T is the operating temperature in Kelvin scale, and e is the elementary charge. The extracted Coulombic capture radius with corresponding dielectric constanst for all devices are presented in Table 4. In OSCs, generated excitons are initially binded together before the dissociation which is defined as the Coulomb binding. Only when the distance bewteen charge carriers exceed the Coulombic capture radius, the exciton can be dissociated [46]. A large Coulombic capture radius indicates that the excitions are more difficult to be dissociated. From Table 4, both photo-degraded and thermal-degraded devices were found possess an increased R_c value compared to fresh devices. In addtion, the increasement was found much larger in photo-degraded devices for both fullerene and non-fullerene based devices. The results implied that the reduction in exciton dissociation ability is more dependent on the fast inital photo degradation rather than the fast inital thermal degradation.

Steady-state photoluminescence (PL) was performed for all devices in order to gain deeper insights into the degradation mechanism. The normalized PL spectrums were shown in Figure 8. It is obvious to see that, for both fullerene and non-fullerene based, photo-degraded devices showed a dramtically increased PL intensity, while the PL intensity of thermal-degraded devices is almost unchanged when comparing to fresh devices. The PL intensity from the

steady-state PL is usually related to the number of excitons in organic solar cells. The high PL intensity indicates a large number of excitons exists in the active layer [47, 48]. The low PL intensity indicates that the excitons are efficiently dissociated to charge carriers [49, 50]. Thus, a significantly increased PL intensity implies a largely decreased exciton dissociation ability for photo-degraded devices which is considered as one of the main reason for the fast inital photo degradation. Herein, the observation is consistent with the results obtained from C-V charactersation. On the other hand, time-resolved photoluminescence (TRPL) was conducted to investigate the dynamics of fast inital photo degradation and thermal degradation for fresh, photo-degraded and thermal-degraded, both fullerene and non-fullerene based devices. Figure 9 showed the TRPL decay curve under the 532 nm light excitation, and a bi-exponential decay model below was used to simulate the curve and extract the excited state lifetime [51]:

$$Y = A_1 \exp\left(-\frac{t}{\tau_1}\right) + A_2 \exp\left(-\frac{t}{\tau_2}\right) + y_0 \qquad (6)$$

where A_1 and A_2 represent the amplitudes and τ_1 and τ_2 represent the fast and slow lifetimes for the carrier recombination. Table 5 listed the obtained excited lifetime values for all devices. It can be seen that both photo-degraded and thermal-degraded devices showed an increased excited lifetime compared to fresh devices. Neverthless, for both fullerene and non-fullerene based, photo-degraded devices showed a much larger increasement in fast and long excited lifetime than thermal-degraded devices. Excited lifetime can indicate the energy and carrier transfer process inside the active layer which is corresponded with the potential of the heterojunction [52]. Since the förster resonance energy transfer (FRET) offers an alternative non-radiative pathway between the donor and acceptor, the excited state lifetime can be used to evaluate the energy transfer process in the active layer [53]. The higher exited state lifetime usually represents a more inefficient energy transfer. Herein, fast inital photo degradation was found to have a larger negative impact on energy transfer process compared to fast inital thermal degradation. This is in accordant with the higher V_{oc} loss observed in photo-degraded devices. The degraded energy transfer ability was identified as one of the main reasons for the fast inital photo degradation but less related to fast inital thermal degradation.

A diode ideality factor (n) and carrier recombination resistance (R_{rec}) analysis were performed to investigate the non-radiative recombination changes during the fast inital degradation. According to the ideal diode model, the diode ideality factor can be estimated from the slope in the exponential region of dark J-V curves (shown in Figure 5) by using the equation below [54]:

$$n = \frac{q}{kT} \frac{dV_{bias}}{dln(J_D)} \qquad (7)$$

With regarding dark J-V curves, the differential diode ideality factor at each voltage was calculated out and depicted in Figure 10 (a) and (b) for fullerene and non-fullerene based devices, respectively.

When the external bias voltage exceeds 0.6 V, dark J-V curves have an exponential region with the parasitic effects occurred [55, 56]. Under a high voltage bias, when the minimum differential diode ideality factor value is very sharp, parastic resistance hardly allow to correctly determine the intrinsic diode ideality factor as the recombination-limited slope is not reached [54]. Thus, this minmum value is considered as the upper limit of the differential diode ideality factor. The dash lines in Figure 10 represent this upper limit as well as the estmated diode ideality factor for all devices. As obtained the diode ideality factor, the carrier recombination resitance (R_{rec}) which is related to the non-radiative recombination process then can be calculated by using the following equation [57]:

$$R_{rec} = \frac{V_e}{J_{sc}} \left(e^{\frac{q(V_{OC} - V_e - B)}{nKT}} \right) \qquad (8)$$

where V_e is the effective voltage for the minmum ideality factor and $B = J_{sc}R_s$ which represents the voltage loss across the series resistance. Since extracted from the dark J-V which is meausure under the dark condtion without light generation, R_{rec} can reasonbale explain the non-radative recombintion in the device [58, 59]. The high R_{rec} indicates a high ability to resist non-radiative recombination [57, 58]. The extracted n and R_{rec} value for both fullerene and non-fulleren based, fresh, photo-degraded and thermal-degraded devices are listed in Table 6, and the coresponding calculation parameters including V_e, R_s and B is shown in Table S3. From Table 6, after 5 hours degradation, both photo-degraded and thermal-degraded devices were observed a reduction in carrier recombination resistance compared to fresh devices. Nevertheless, this reduction was found much larger in photo-degraded devices for both fullerene and non-fullerene based devices. The results revealed that fast inital photo degradation has a stronger negative impact on the the non-radiative recombinaiton in the device.

AFM and SEM characterisations were conducted to investigate the morphology changes during the fast inital degradation. AFM images were shown in Figure 11 ,and SEM images were shown in Figure S1 for both fulleren and non-fullerene based fresh, photo-degraded and thermal-degraded devices. In addtion, the root-mean roughness (RMS) values estimated are shown in each corresponding image. It was found that the RMS value for both photo-degraded and

thermal degraded devices is larger than the value of the fresh device. For fulleren based devices, the RMS value increased from 3.65 nm to 5.35 nm and 5.00 nm after 5 hours fast inital photo and thermal degradation respectively. Similarly, for non-fullerene based devices, the RMS value increased from 4.24 nm to 4.98 nm and 4.34 nm after the fast inital photo and thermal degradation. Apparently, the fast inital photo degradaiton was found to induce a higher extent of roughness than fast inital thermal degradation. The high RMS value with rougher surface morphology implies a strong aggregation behaviour inside the active layer which related to a large phase separated domains with more traps. It can negatively affect charge dissociation process and increase the non-radiative recombination in the device [60, 61]. Hence, the decreased charge dissociation and increased non-radaitive recombinaiton were found as two major degrdation reasons for the fast inital photo degradation. Herein, the result is consistent with the the steady-state PL results, the diode ideality factor analysis and carrier recombination resistance analysis.

Overall, although a similar device PCE drop was observed from the fast inital photo and thermal degradation for both types of devices, the mechanism behind these two types of degradation was found different. Urbach energy estimation pointed out that both photo and thermal degradation can cause an increased energetic disorder with a higher trap mediated charge recombination. Meanwhile, steady-state PL, TRPL and C-V measurements indicate that the fast inital photo degradation is more dominated by degraded charge dissociation ability and energy transfer ability compared to fast inital thermal degradation. Moreover, carrier recombination resistance estimation and AFM characterisation found that photo degradation caused a relative stronger negative impact on the non-radiative recombination in the fast inital process. However, the dark J-V measurement and the J_{sat} with P analysis showed that the fast inital thermal degradation is more related to the increased leakage potential and degraded current extraction process compared to fast inital photo degradation.

4. Conclusion

In summary, we studied and compared the fast inital photo degradation and fast inital thermal degradation for both PTB7-Th:PC$_{71}$BM fullerene based and PTB7-Th:ITIC non-fullerene based devices. The Urbach energy determined indicates that both photo and thermal degradaiton during the fast inital process can cause energy disorder. However, the fast inital photo and thermal degradaiton were identified have a very different machansim. Compared to

the fast inital thermal degradation, fast inital photo degradation was found has more negative effects on the energy transfer process and exition dissciation process and caused a higher increase in non-radiative recombination. Differently, the fast inital thermal degradation was found more responsible for the degradation in the current extraction process and can induce a higher current leakage potential. As the organic solar cell emerging as one of the promising energy technologies, it becomes essential to address its stability issue. Understanding the mechanism behind the fast inital degradation process thus is a crucial step towards further development and commercialization.

Acknowledgement

Funding declaration

Supporting Information

Statistical PV parameters for planar perovskite solar cell device in sun light, Transmittance, Reflectance and External Quantum Efficiency measurements, EDX and SEM images, Schematic design of the indoor system, LED light spectrum, EQE for indoor, J-V curve at constant bias near the maximum power point, summarized averages of the PV parameters under illumination of both sun and indoor light, statistical PV parameters for planar perovskite solar cell device in indoor light.

References

1. M. Kaltenbrunner, M. S. White, E. D. Głowacki, T. Sekitani, T. Someya, N. S. Sariciftci and S. Bauer, *Nature Communications*, 2012, **3**, 770.

2. Q.-D. Ou, H.-J. Xie, J.-D. Chen, L. Zhou, Y.-Q. Li and J.-X. Tang, *Journal of Materials Chemistry A*, 2016, **4**, 18952-18962.

3. M. B. Upama, M. Wright, N. K. Elumalai, M. A. Mahmud, D. Wang, K. H. Chan, C. Xu, F. Haque and A. Uddin, *Current Applied Physics*, 2017, **17**, 298-305.

4. W. Yu, X. Jia, Y. Long, L. Shen, Y. Liu, W. Guo and S. Ruan, *ACS Applied Materials & Interfaces*, 2015, **7**, 9920-9928.

5. C. Yan, S. Barlow, Z. Wang, H. Yan, A. K. Y. Jen, S. R. Marder and X. Zhan, *Nature Reviews Materials*, 2018, **3**, 18003.

6. W. Chen and Q. Zhang, *Journal of Materials Chemistry C*, 2017, **5**, 1275-1302.

7. B. Jia, Y. Wu, F. Zhao, C. Yan, S. Zhu, P. Cheng, J. Mai, T.-K. Lau, X. Lu, C.-J. Su, C. Wang and X. Zhan, *Science China Chemistry*, 2017, **60**, 257-263.

8. M. Privado, V. Cuesta, P. de la Cruz, M. L. Keshtov, G. D. Sharma and F. Langa, *Journal of Materials Chemistry A*, 2017, **5**, 14259-14269.

9. Y. Lin, J. Wang, Z.-G. Zhang, H. Bai, Y. Li, D. Zhu and X. Zhan, *Advanced Materials*, 2015, **27**, 1170-1174.

10. H. Li, Z. Xiao, L. Ding and J. Wang, *Science Bulletin*, 2018, **63**, 340-342.

11. L. Meng, Y. Zhang, X. Wan, C. Li, X. Zhang, Y. Wang, X. Ke, Z. Xiao, L. Ding, R. Xia, H.-L. Yip, Y. Cao and Y. Chen, *Science*, 2018, DOI: 10.1126/science.aat2612.

12. Z. Xiao, X. Jia and L. Ding, *Science Bulletin*, 2017, **62**, 1562-1564.

13. Z. Xiao, X. Jia, D. Li, S. Wang, X. Geng, F. Liu, J. Chen, S. Yang, T. P. Russell and L. Ding, *Science Bulletin*, 2017, **62**, 1494-1496.

14. C. Xu, M. Wright, D. Ping, H. Yi, X. Zhang, M. D. A. Mahmud, K. Sun, M. B. Upama, F. Haque and A. Uddin, *Organic Electronics*, 2018, **62**, 261-268.

15. M. O. Reese, S. A. Gevorgyan, M. Jørgensen, E. Bundgaard, S. R. Kurtz, D. S. Ginley, D. C. Olson, M. T. Lloyd, P. Morvillo, E. A. Katz, A. Elschner, O. Haillant, T. R. Currier, V. Shrotriya, M. Hermenau, M. Riede, K. R. Kirov, G. Trimmel, T. Rath, O. Inganäs, F. Zhang, M. Andersson, K. Tvingstedt, M. Lira-Cantu, D. Laird, C. McGuiness, S. Gowrisanker, M. Pannone, M. Xiao, J. Hauch, R. Steim, D. M. DeLongchamp, R. Rösch, H. Hoppe, N. Espinosa, A. Urbina, G. Yaman-Uzunoglu, J.-B. Bonekamp, A. J. J. M. van Breemen, C. Girotto, E. Voroshazi and F. C. Krebs, *Solar Energy Materials and Solar Cells*, 2011, **95**, 1253-1267.

16. M. B. Upama, N. K. Elumalai, M. A. Mahmud, H. Sun, D. Wang, K. H. Chan, M. Wright, C. Xu and A. Uddin, *Thin Solid Films*, 2017, **636**, 127-136.

17. M. B. Upama, M. Wright, M. A. Mahmud, N. K. Elumalai, A. Mahboubi Soufiani, D. Wang, C. Xu and A. Uddin, *Nanoscale*, 2017, **9**, 18788-18797.

18. M. B. Upama, M. Wright, B. Puthen-Veettil, N. K. Elumalai, M. A. Mahmud, D. Wang, K. H. Chan, C. Xu, F. Haque and A. Uddin, *RSC Advances*, 2016, **6**, 103899-103904.

19. Q. Burlingame, X. Tong, J. Hankett, M. Slootsky, Z. Chen and S. R. Forrest, *Energy & Environmental Science*, 2015, **8**, 1005-1010.

20. A. Manor, E. A. Katz, T. Tromholt and F. C. Krebs, *Advanced Energy Materials*, 2011, **1**, 836-843.

21. G. Garcia-Belmonte, P. P. Boix, J. Bisquert, M. Sessolo and H. J. Bolink, *Solar Energy Materials and Solar Cells*, 2010, **94**, 366-375.

22. S. J. Ikhmayies and R. N. Ahmad-Bitar, *Journal of Materials Research and Technology*, 2013, **2**, 221-227.

23. Z. Kam, X. Wang, J. Zhang and J. Wu, *ACS Applied Materials & Interfaces*, 2015, **7**, 1608-1615.

24. C. Yan, K. Sun, J. Huang, S. Johnston, F. Liu, B. P. Veettil, K. Sun, A. Pu, F. Zhou, J. A. Stride, M. A. Green and X. Hao, *ACS Energy Letters*, 2017, **2**, 930-936.
25. C.-P. Chen, Y.-Y. Tsai, Y.-C. Chen and Y.-H. Li, *Solar Energy*, 2018, **176**, 170-177.
26. I. Gur, N. A. Fromer, M. L. Geier and A. P. Alivisatos, *Science*, 2005, **310**, 462-465.
27. W. Ma, C. Yang, X. Gong, K. Lee and A. J. Heeger, *Advanced Functional Materials*, 2005, **15**, 1617-1622.
28. Y. Sun, C. J. Takacs, S. R. Cowan, J. H. Seo, X. Gong, A. Roy and A. J. Heeger, *Advanced Materials*, 2011, **23**, 2226-2230.
29. L. Krishnan Jagadamma, M. T. Sajjad, V. Savikhin, M. F. Toney and I. D. W. Samuel, *Journal of Materials Chemistry A*, 2017, **5**, 14646-14657.
30. E. A. Katz, A. Mescheloff, I. Visoly-Fisher and Y. Galagan, *Solar Energy Materials and Solar Cells*, 2016, **144**, 273-280.
31. Z. He, B. Xiao, F. Liu, H. Wu, Y. Yang, S. Xiao, C. Wang, T. P. Russell and Y. Cao, *Nature Photonics*, 2015, **9**, 174.
32. N. Jain, N. Chandrasekaran, A. Sadhanala, R. H. Friend, C. R. McNeill and D. Kabra, *Journal of Materials Chemistry A*, 2017, **5**, 24749-24757.
33. W. Gong, M. A. Faist, N. J. Ekins-Daukes, Z. Xu, D. D. C. Bradley, J. Nelson and T. Kirchartz, *Physical Review B*, 2012, **86**, 024201.
34. F. Urbach, *Physical Review*, 1953, **92**, 1324-1324.
35. J. Lee, K. Vandewal, S. R. Yost, M. E. Bahlke, L. Goris, M. A. Baldo, J. V. Manca and T. Van Voorhis, *Journal of the American Chemical Society*, 2010, **132**, 11878-11880.
36. R. A. Street, K. W. Song, J. E. Northrup and S. Cowan, *Physical Review B*, 2011, **83**, 165207.
37. C. H. Peters, I. T. Sachs-Quintana, W. R. Mateker, T. Heumueller, J. Rivnay, R. Noriega, Z. M. Beiley, E. T. Hoke, A. Salleo and M. D. McGehee, *Advanced Materials*, 2012, **24**, 663-668.
38. M. A. Mahmud, N. K. Elumalai, M. Upama, D. Wang, F. Haque, M. Wright, C. Xu and A. Uddin, *Solar energy and solar materials*, 2017, **167,** 70-86.
39. C. M. Proctor, M. Kuik and T.-Q. Nguyen, *Progress in Polymer Science*, 2013, **38**, 1941-1960.
40. M. Lenes, M. Morana, C. J. Brabec and P. W. M. Blom, *Advanced Functional Materials*, 2009, **19**, 1106-1111.
41. C. G. Shuttle, A. Maurano, R. Hamilton, B. O'Regan, J. C. d. Mello and J. R. Durrant, *Applied Physics Letters*, 2008, **93**, 183501.
42. W. Tress, S. Corvers, K. Leo and M. Riede, *Advanced Energy Materials*, 2013, **3**, 873-880.
43. Y. Zhao, Z. Xie, C. Qin, Y. Qu, Y. Geng and L. Wang, *Solar Energy Materials and Solar Cells*, 2009, **93**, 604-608.
44. T. Schiros, G. Kladnik, D. Prezzi, A. Ferretti, G. Olivieri, A. Cossaro, L. Floreano, A. Verdini, C. Schenck, M. Cox, A. A. Gorodetsky, K. Plunkett, D. Delongchamp, C. Nuckolls, A. Morante, D. Cvetko and I. Kymissis, *Advanced Energy Materials*, 2013, **3**, 894-902.
45. C. Zhan, X. Zhang and J. Yao, *RSC Advances*, 2015, **5**, 93002-93026.
46. S. N. Hood and I. Kassal, *The Journal of Physical Chemistry Letters*, 2016, **7**, 4495-4500.
47. B. Arredondo, B. Romero, G. Del Pozo, M. Sessler, C. Veit and U. Würfel, *Solar Energy Materials and Solar Cells*, 2014, **128**, 351-356.
48. S. Holliday, R. S. Ashraf, A. Wadsworth, D. Baran, S. A. Yousaf, C. B. Nielsen, C.-H. Tan, S. D. Dimitrov, Z. Shang, N. Gasparini, M. Alamoudi, F. Laquai, C. J. Brabec, A. Salleo, J. R. Durrant and I. McCulloch, *Nature Communications*, 2016, **7**, 11585.
49. M. Upama, N. K. Elumalai, M. A. Mahmud, M. Wright, D. Wang, C. Xu, F. Haque, K. Howe Chan and A. Uddin, *Applied Surface Science*, 2017, **416**, 834-884.
50. S. L. M. van Mensfoort and R. Coehoorn, *Physical Review Letters*, 2008, **100**, 086802.
51. D. Bi, C. Yi, J. Luo, J.-D. Décoppet, F. Zhang, S. M. Zakeeruddin, X. Li, A. Hagfeldt and M. Grätzel, *Nature Energy*, 2016, **1**.
52. P. W. Liang, C. Y. Liao, C. C. Chueh, F. Zuo, S. T. Williams, X. K. Xin, J. Lin and A. K. Jen, *Adv Mater*, 2014, **26**, 3748-3754.

53. A. A. Mohapatra, V. Kim, B. Puttaraju, A. Sadhanala, X. Jiao, C. R. McNeill, R. H. Friend and S. Patil, *ACS Applied Energy Materials*, 2018, **1**, 4874-4882.

54. W. Tress, M. Yavari, K. Domanski, P. Yadav, B. Niesen, J. P. Correa Baena, A. Hagfeldt and M. Graetzel, *Energy & Environmental Science*, 2018, **11**, 151-165.

55. T. Kirchartz, F. Deledalle, P. S. Tuladhar, J. R. Durrant and J. Nelson, *The Journal of Physical Chemistry Letters*, 2013, **4**, 2371-2376.

56. G. A. H. Wetzelaer, M. Kuik, M. Lenes and P. W. M. Blom, *Applied Physics Letters*, 2011, **99**, 153506.

57. L. Duan, H. Yi, C. Xu, M. B. Upama, M. A. Mahmud, D. Wang, F. H. Shabab and A. Uddin, *IEEE Journal of Photovoltaics*, 2018, DOI: 10.1109/jphotov.2018.2870722, 1-9.

58. B. Arredondo, M. B. Martín-López, B. Romero, R. Vergaz, P. Romero-Gomez and J. Martorell, *Solar Energy Materials and Solar Cells*, 2016, **144**, 422-428.

59. F. Haque, M. Wright, M. A. Mahmud, H. Yi, D. Wang, L. Duan, C. Xu, M. B. Upama and A. Uddin, *ACS Omega*, 2018, **3**, 11937-11944.

60. Q. An, F. Zhang, L. Li, J. Wang, J. Zhang, L. Zhou and W. Tang, *ACS Applied Materials & Interfaces*, 2014, **6**, 6537-6544.

61. J. Wan, X. Xu, G. Zhang, Y. Li, K. Feng and Q. Peng, *Energy & Environmental Science*, 2017, **10**, 1739-1745.
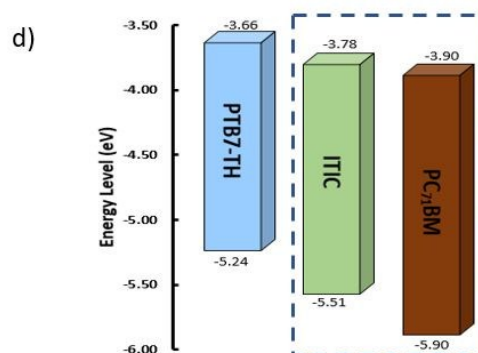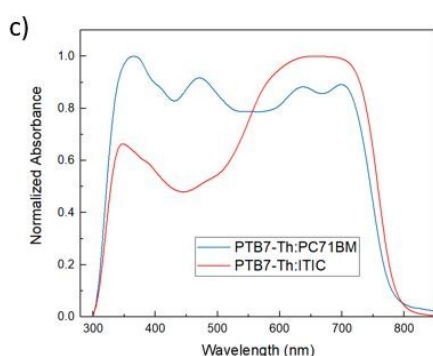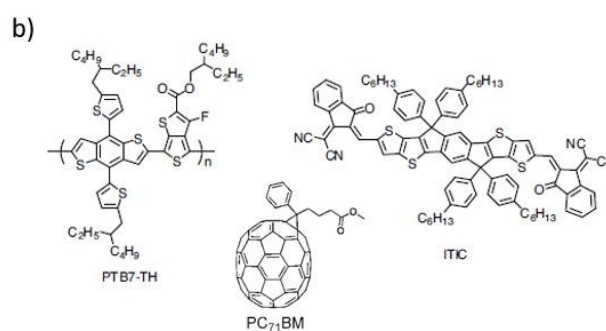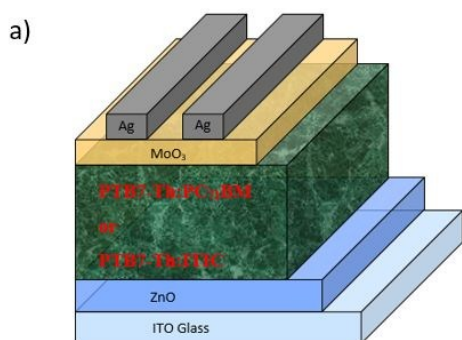
Figure 1. a) Schematic diagram of device structures of both fullerene-based and non-fullerene-based organic solar cells. b) Chemical structures of donor material PTB7-Th and acceptor materials ITIC and $PC_{71}BM$. c) The normalised absorbance spectrum of PTB7-Th:$PC_{71}BM$ and PTB7-Th:ITIC blend. d) Energy band diagrams of donor material PTB7-Th and acceptor materials ITIC and $PC_{71}BM$.
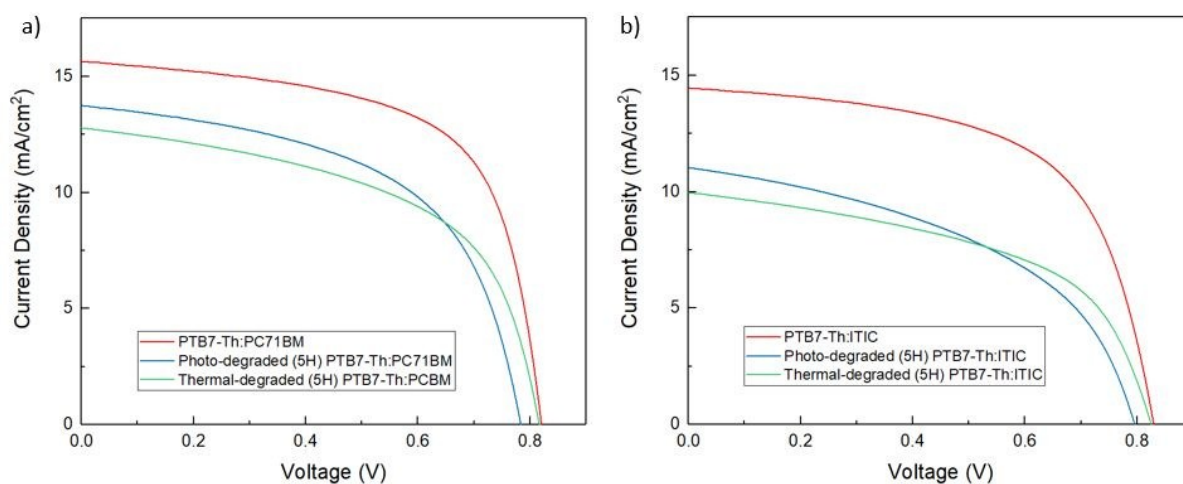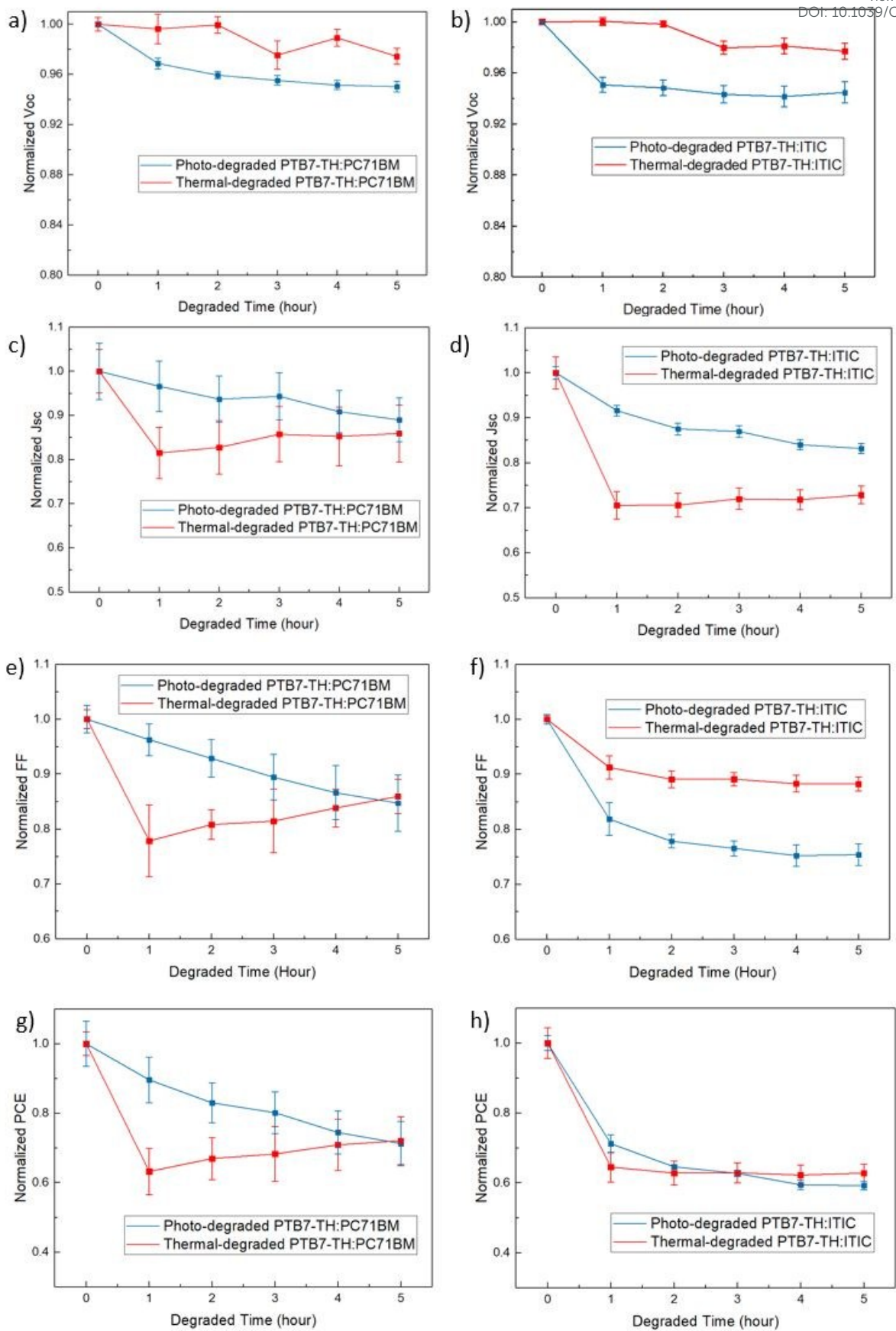
Figure 2. Current-voltage (J-V) characteristics of the fabricated solar cells both a) PTB7-Th:$PC_{71}BM$ fullerene based and b) PTB7-Th:ITIC non-fullerene based, fresh, photo-degraded thermal-degraded devices at room temperature under one-sun test condition (AM1.5 G illumination at 100 mW/cm^2).
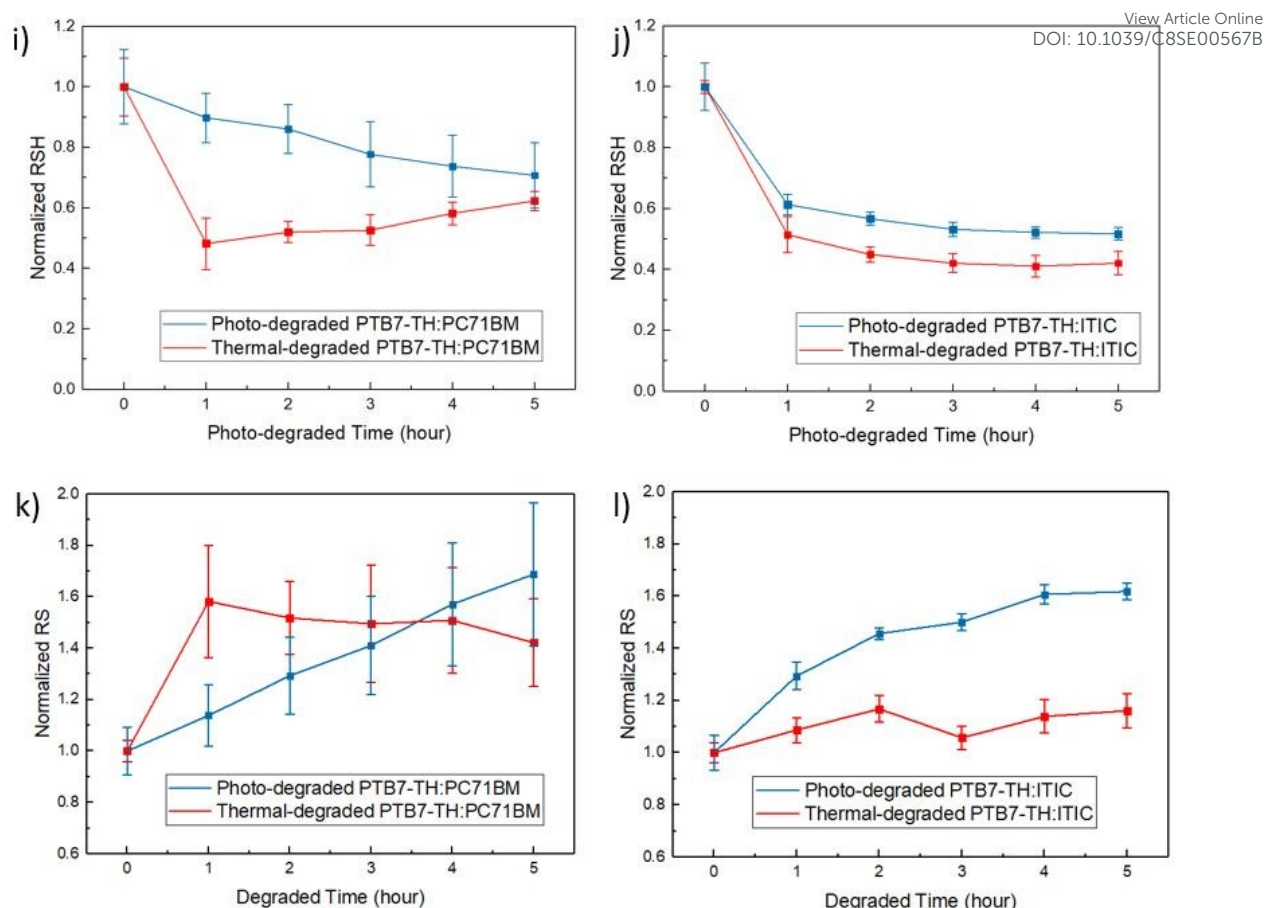
Figure 3. Normalized photovoltaic parameters including open circuit voltage (V_{oc}), short circuit current (J_{sc}), fill factor (FF), power conversion efficiency (PCE), shun resistance (R_{sh}) and series resistance (R_s) for 5 hours of continuous light illumination under one-sun test condition (AM1.5G illumination at 100 mW cm^{-2}) for fullerene and non-fullerene based devices; a) and b) Voc, c) and d) Jsc, e) and f) FF, g) and h) PCE, i) and j)R_{sh}, and k) and l) R_s versus time.
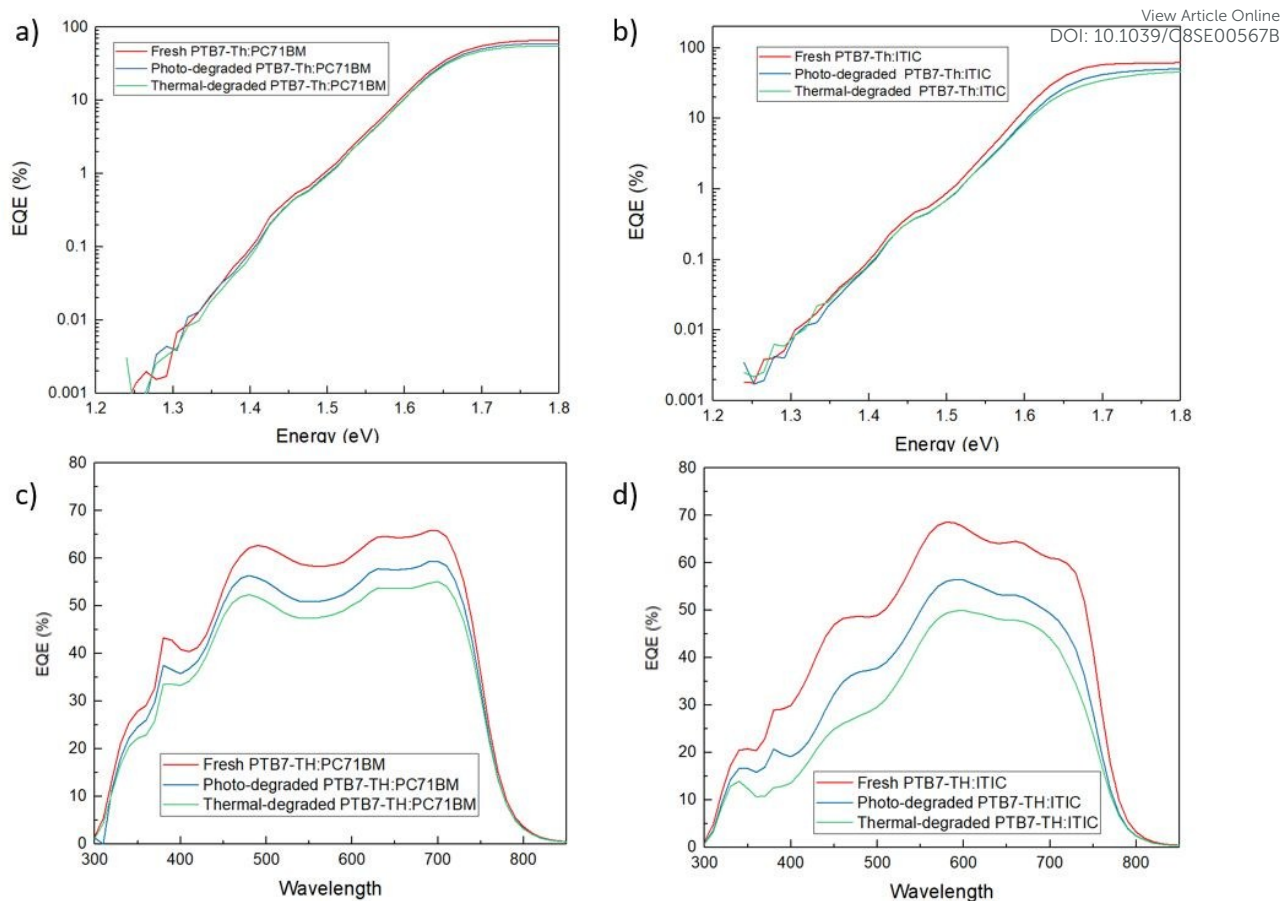
Figure 4. External quantum efficiency (EQE) spectrum versus the incident photo energy for a) PTB7-Th:PC$_{71}$BM fullerene and b) PTB7-Th:ITIC non-fullerene based fresh, photo-degraded and thermal-degraded devices. External quantum efficiency (EQE) spectrum versus light wavelength for c) PTB7-Th:PC$_{71}$BM fullerene and d) PTB7-Th:ITIC non-fullerene based fresh, photo-degraded and thermal-degraded devices.
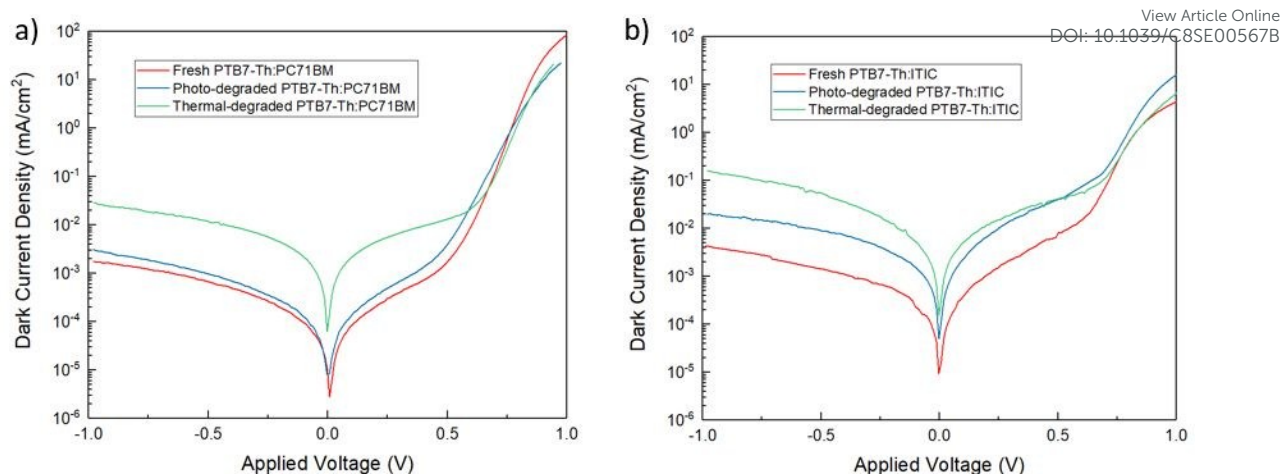
Figure 5. Dark Current-voltage characteristics of the fabricated solar cells for a) PTB7-Th:PC$_{71}$BM fullerene and b) PTB7-Th:ITIC non-fullerene based fresh, photo-degraded and thermal-degraded devices.
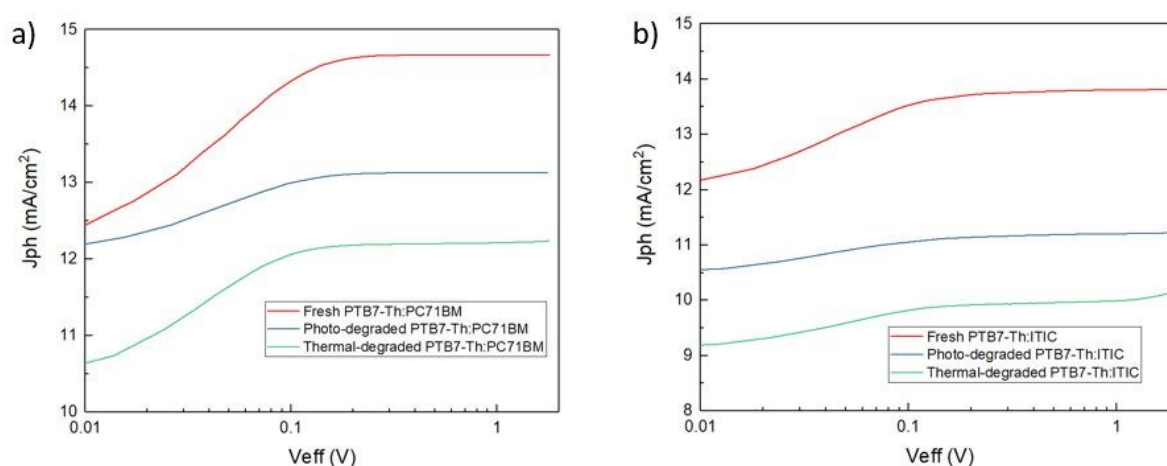
Figure 6. Variation of photocurrent (J$_{ph}$) with effective voltage (V$_{eff}$) for OSCs for a) PTB7-Th:PC$_{71}$BM fullerene and b) PTB7-Th:ITIC non-fullerene based fresh, photo-degraded and thermal-degraded devices.
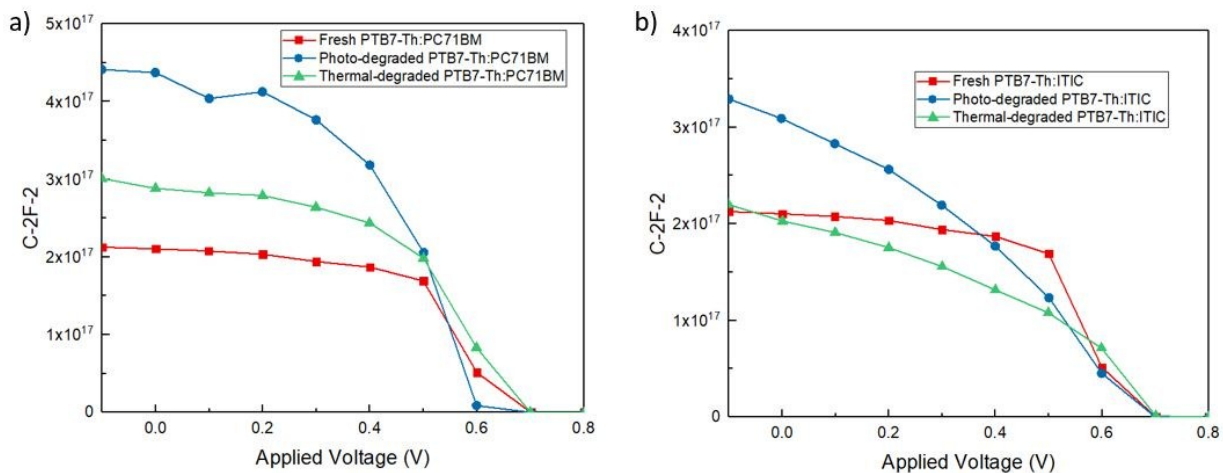
Figure 7. Mott Schottky curves of a) PTB7-Th:PC$_{71}$BM fullerene and b) PTB7-Th:ITIC non-fullerene based, fresh, photo-degraded and thermal-degraded devices at 1 kHz frequency under the dark condition.
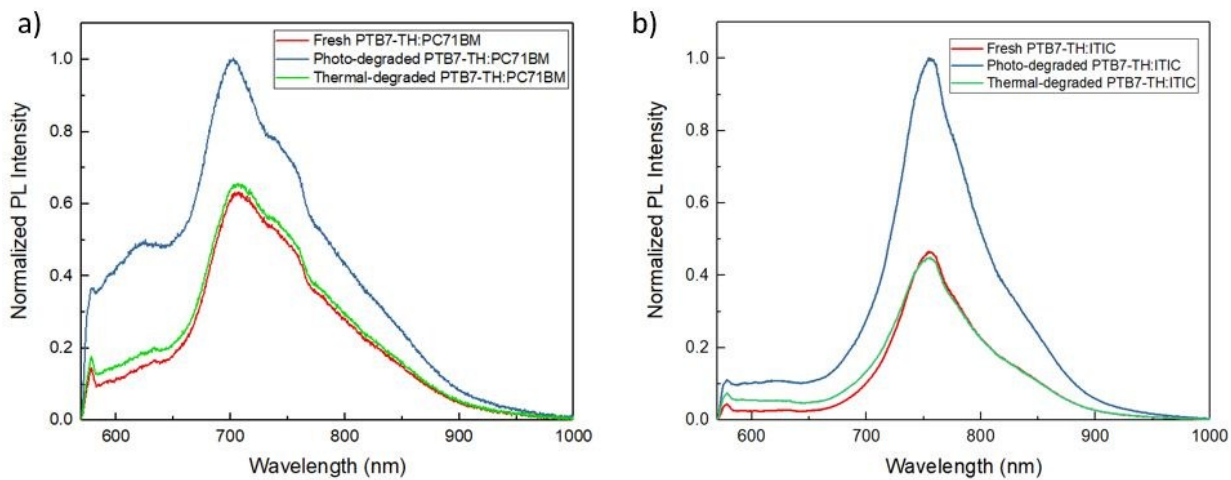

Figure 8. Normalized steady-state photoluminescence (PL) emission spectra of a) PTB7-Th:PC$_{71}$BM fullerene and b) PTB7-Th:ITIC non-fullerene based fresh, photo-degraded and thermal-degraded devices.
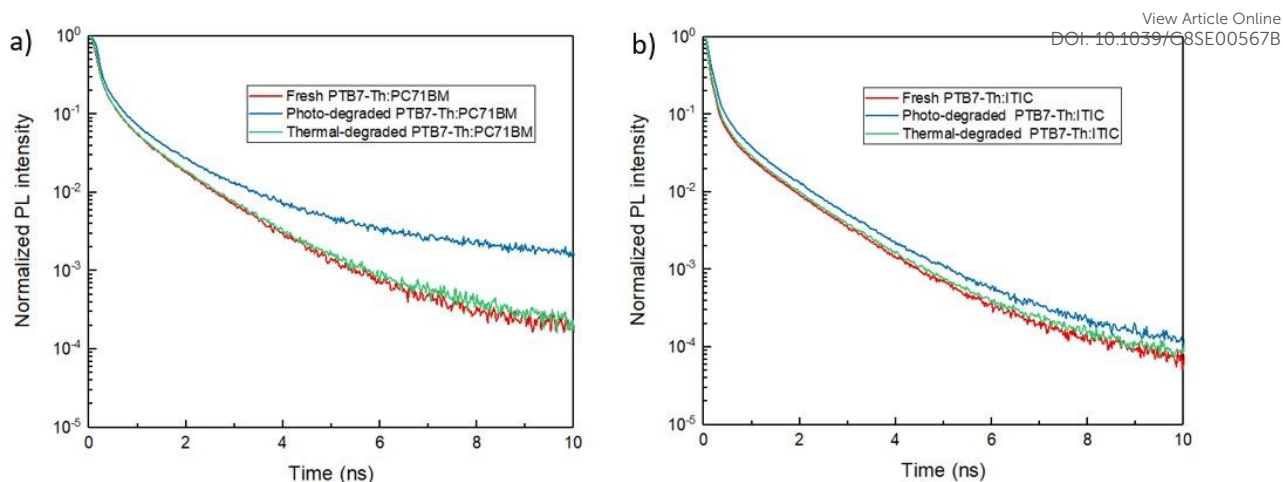
Figure 9. Normalized time-resovled photoluminescence (TRPL) emission spectra of a) PTB7-Th:PC$_{71}$BM fullerene and b) PTB7-Th:ITIC non-fullerene based fresh, photo-degraded and thermal-degraded devices.
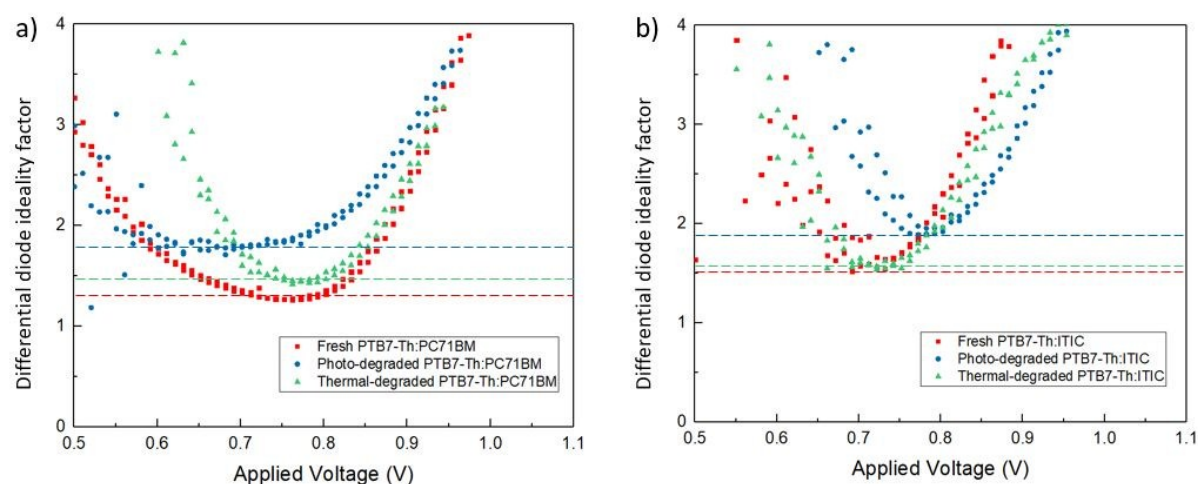

Figure 10. The differential ideality factor calculated from the slope of the dark J-V curves versus the applied voltage bias for a) PTB7-Th:PC$_{71}$BM fullerene and b) PTB7-Th:ITIC non-fullerene based fresh, photo-degraded and thermal-degraded devices.

Figure 11. The AFM images with the RMS value of both PTB7-Th:PC$_{71}$BM fullerene and PTB7-Th:ITIC non-fullerene based, fresh, photo-degraded and thermal-degraded blend films deposited on top of ITO/ZnO surface.

Sustainable Energy & Fuels

Table 1. Photovoltaic parameters including open circuit voltage (V_{oc}), short circuit current (J_{sc}), fill factor (FF), power conversion efficiency (PCE), shun resistance (R_{sh}) and series resistance (R_s) of both PTB7-Th:PC$_{71}$BM fullerene and PTB7-Th:ITIC non-fuller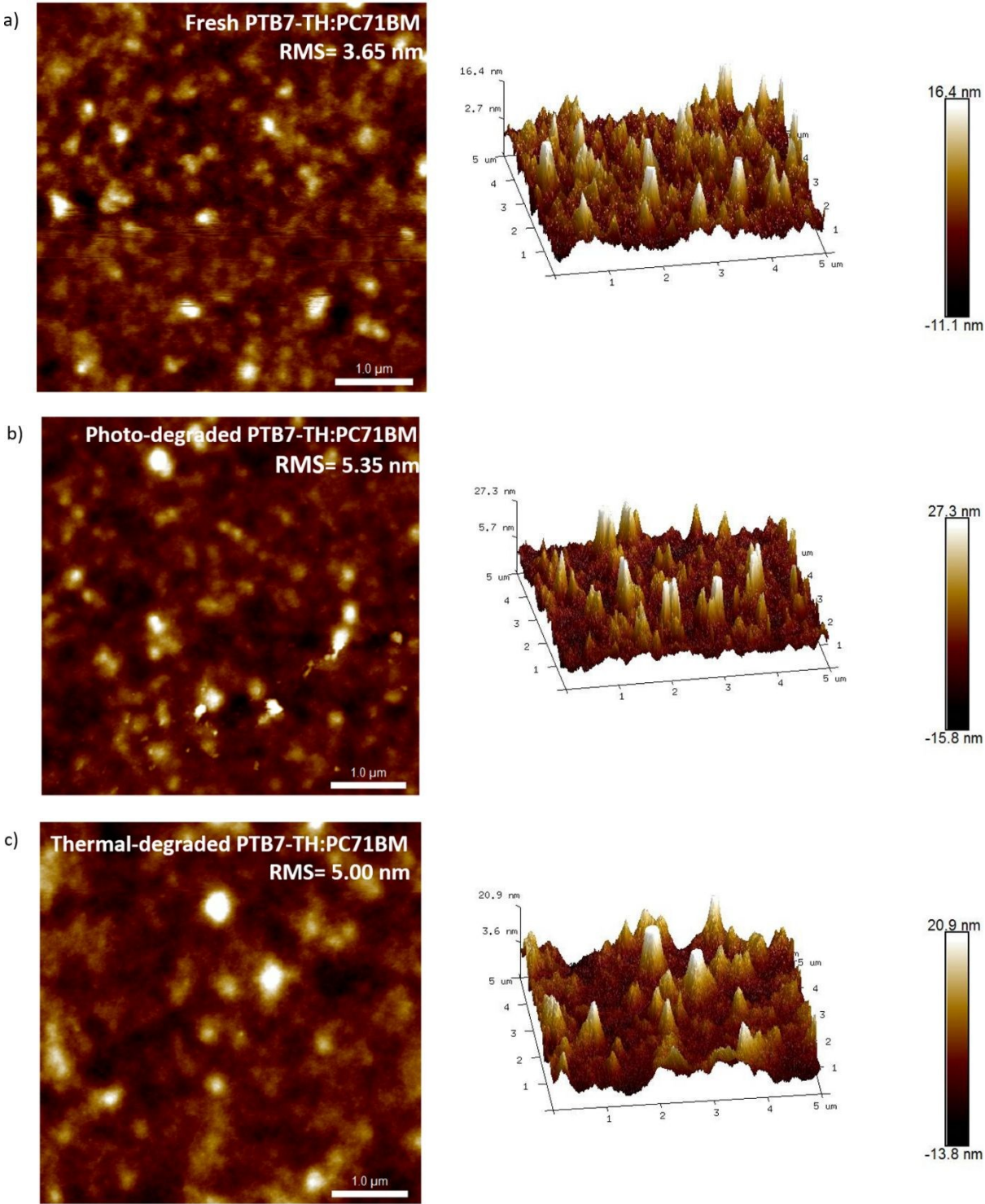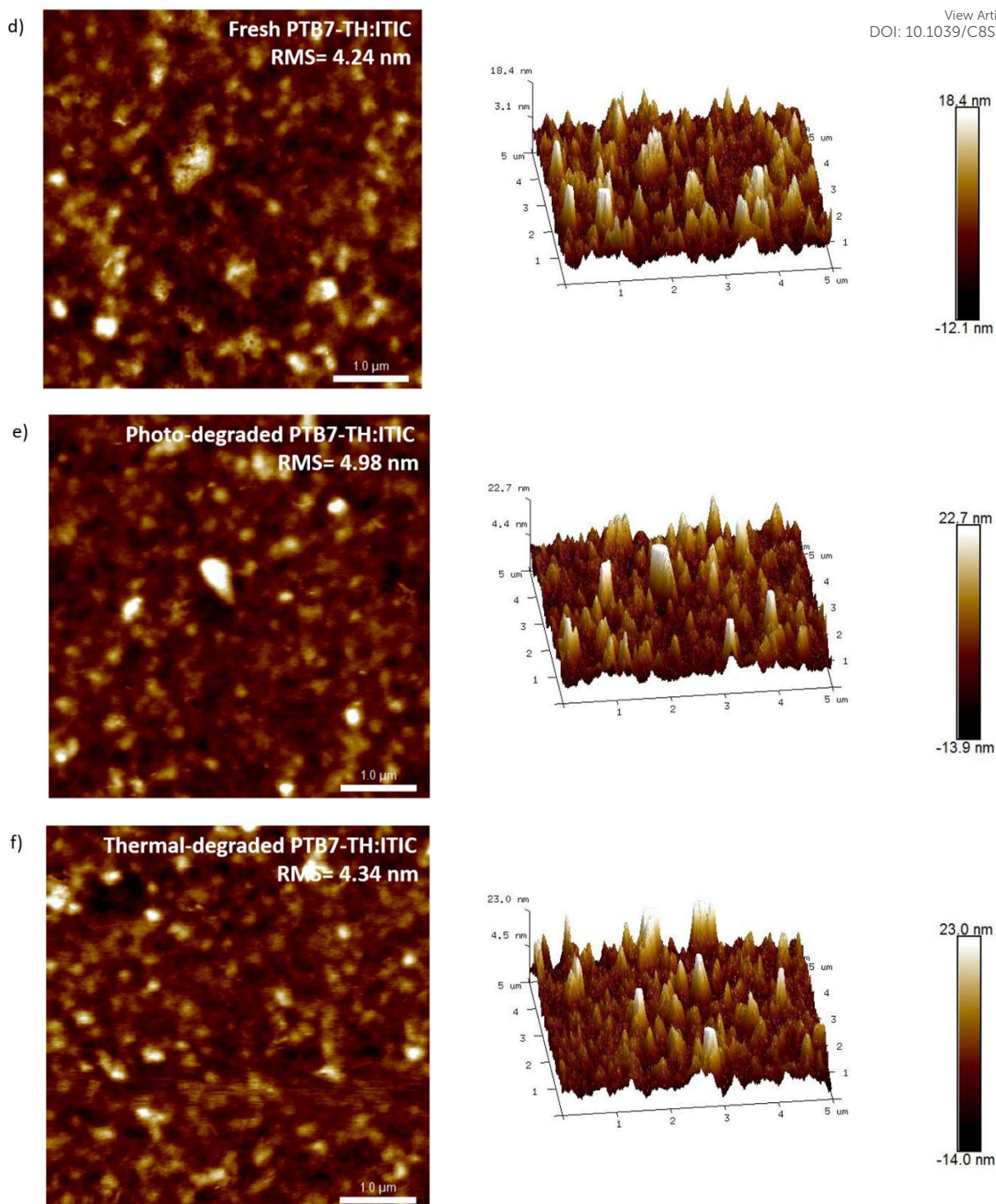ene based fresh, photo-degraded and thermal-degraded devices measured at room temperature under one-sun test condition (AM1.5 G illumination,100 mW/cm^2) obtained from at least 5 devices.

Device	V_{OC} (V)	J_{SC} (mA/cm^2)	FF	Ave PCE	R_{SH} (Ωcm^2)	R_S (Ωcm^2)
Fresh PTB7-Th:PC71BM	0.82 ± 0.003	14.67 ± 0.67	0.61 ± 0.02	7.40 ± 0.34%	541 ± 56	6.07 ± 0.99
Photo-degraded PTB7-Th:PC71BM	0.778 ± 0.003	13.13 ± 0.73	0.53 ± 0.03	5.40 ± 0.48%	406 ± 62	9.65 ± 1.60
Thermal-degraded PTB7-Th:PC71BM	0.800 ± 0.005	12.44 ± 0.94	0.52 ± 0.02	5.22 ± 0.50%	325 ± 17	8.50 ± 1.01
Fresh PTB7-Th:ITIC	0.83 ± 0.002	13.80 ± 0.46	0.60 ± 0.01	6.84 ± 0.26%	644 ± 39	8.36 ± 0.53
Photo-degraded PTB7-Th:ITIC	0.785 ± 0.007	11.20 ± 0.15	0.45 ± 0.01	3.98 ± 0.07%	335 ± 14	13.36 ± 0.27
Thermal-degraded PTB7-Th:ITIC	0.812 ± 0.005	10.02 ± 0.27	0.53 ± 0.01	4.30 ± 0.17%	280 ± 25	9.84 ± 0.55

Table 2. Extracted Urbach energy of both PTB7-Th:PC$_{71}$BM fullerene and PTB7-Th:ITIC non-fullerene based fresh, photo-degraded and thermal-degraded devices.

Device	Urbach Energy (m eV)
Fresh PTB7-Th:PC71BM	45.02
Photo-degraded PTB7-Th:PC71BM	50.27
Thermal-degraded PTB7-Th:PC71BM	50.56
Fresh PTB7-Th:ITIC	54.44
Photo-degraded PTB7-Th:ITIC	58.02
Thermal-degraded PTB7-Th:ITIC	57.21

Table 3. Exciton dissociation probabilities (P) and saturation current density (J_{sat}) of both PTB7-Th:PC$_{71}$BM fullerene and PTB7-Th:ITIC non-fullerene based fresh, photo-degraded and thermal-degraded devices.

Devices	J_{sat} (mA/cm^2)	P (%)
Fresh PTB7-Th:PC71BM	14.67	99.98%
Photo-degraded PTB7-Th:PC71BM	13.13	99.97%
Thermal-degraded PTB7-Th:PC71BM	12.24	99.77%
Fresh PTB7-Th:ITIC	13.82	99.85%
Photo-degraded PTB7-Th:ITIC	11.22	99.82%
Thermal-degraded PTB7-Th:ITIC	10.14	98.42%

Sustainable Energy & Fuels Accepted Manuscript

Table 4. Extracted dielectric parameters of $C_{1\,kHz}$, dielectric constant ε_r, and Coulomb capture radius R_c of both PTB7-Th:PC$_{71}$BM fullerene and PTB7-Th:ITIC non-fullerene based fresh, photo-degraded and thermal-degraded devices from the C-V measurement.

Device	$C_{1\,kHz}$ (nF)	ε_r	R_c (nm)
Fresh PTB7-Th:PC71BM	2.18	5.47	10.23
Photo-degraded PTB7-Th:PC71BM	1.57	3.95	14.16
Thermal-degraded PTB7-Th:PC71BM	1.88	4.72	11.85
Fresh PTB7-Th:ITIC	2.18	5.47	10.23
Photo-degraded PTB7-Th:ITIC	1.88	4.72	11.86
Thermal-degraded PTB7-Th:ITIC	2.13	5.35	10.45

Table 5. Extracted short and long lifetime for both PTB7-Th:PC$_{71}$BM fullerene and PTB7-Th:ITIC non-fullerene based fresh, photo-degraded and thermal-degraded devices from the normalized TRPL curves by fitting with the bi-exponential decay equation.

Devices	Short Lifetime τ_1 (ns)	Long Lifetime τ_2 (ns)
Fresh PTB7-Th:PC71BM	0.150	1.008
Photo-degraded PTB7-Th:PC71BM	0.190	1.417
Thermal-degraded PTB7-Th:PC71BM	0.162	1.152
Fresh PTB7-Th:ITIC	0.095	0.839
Photo-degraded PTB7-Th:ITIC	0.129	1.007
Thermal-degraded PTB7-Th:ITIC	0.103	0.884

Table 6. Estimated diode ideality factor n and carrier recombination resistance R_{rec} for both PTB7-Th:PC$_{71}$BM fullerene and PTB7-Th:ITIC non-fullerene based fresh, photo-degraded and thermal-degraded devices.

Devices	n	R_{rec} (Ωcm^2)
Fresh PTB7-Th:PC71BM	1.27	278.55
Photo-degraded PTB7-Th:PC71BM	1.71	70.97
Thermal-degraded PTB7-Th:PC71BM	1.44	143.82
Fresh PTB7-Th:ITIC	1.52	1190.28
Photo-degraded PTB7-Th:ITIC	1.89	393.79
Thermal-degraded PTB7-Th:ITIC	1.54	735.68

Comparative study of light and thermal induced degradation for both fullerene and non-fullerene based organic solar cells

Graphical Abstract